

Atomic Scale Characterization of Supported Pd–Cu/ γ -Al₂O₃ Bimetallic Catalysts

K. Sun*

Department of Physics, University of Illinois at Chicago, 845 West Taylor Street, Chicago, Illinois 60607-7059

J. Liu

Monsanto Company, 800 North Lindbergh Boulevard, St. Louis, Missouri 63167

N. K. Nag

Engelhard Corporation, Process Technology Group, 23800 Mercantile Road, Beachwood, Ohio 44122

N. D. Browning

Department of Physics, University of Illinois at Chicago, 845 West Taylor Street, Chicago, Illinois 60607-7059

Received: July 23, 2002; In Final Form: September 18, 2002

The reduction behavior of a Pd–Cu/ γ -Al₂O₃ catalyst precursor (containing 2% Pd and 1% Cu) is studied by atomic scale Z-contrast imaging, electron energy-loss spectroscopy (EELS), and X-ray energy dispersive spectroscopy (EDS) techniques available in a scanning transmission electron microscope (STEM). We found that the alloying behavior of the bimetallic nanoparticles strongly depends on the reduction temperature of the catalyst precursor materials. When the precursor is reduced at 523 or 773 K, individual metallic nanoparticles are formed with a composition varying from pure metallic Pd to Pd–Cu bimetallic alloys. Detailed spectroscopic analyses of the individual nanoparticles show that Pd is preferentially segregated onto the surfaces of the bimetallic Pd–Cu nanoparticles. At higher reduction temperatures, e.g., at 1073 K, however, all the nanoparticles are found to be bimetallic Pd–Cu alloys with either Pd- or Cu-rich surfaces.

1. Introduction

Alloying is a well-known, but poorly understood, phenomenon that can either improve the catalytic properties of the original single-metal catalysts or create new properties which may not be achieved by either of the individual metal catalysts.¹ Supported Pd–Cu bimetallic catalysts are among those systems in which the structural/compositional properties of the bimetallic clusters as well as their catalytic properties have been extensively studied.² The high level of interest in this class of catalysts is partly due to their potential applications in the destruction of nitrates and nitrites.^{3,4} In addition, they can also be used in CO oxidation,⁵ catalytic combustion of methane,⁶ and as auto-exhaust catalysts.⁷

To better understand the catalytic properties of supported bimetallic catalysts, it is necessary to understand both the chemical states and the distribution of the two metals within the individual nanoparticles (e.g., alloying vs segregation).^{2,8,9} While it is commonly believed that elemental segregation can occur on the surfaces of bimetallic nanoparticles particles, the reported results on supported Pd–Cu bimetallic catalysts are inconclusive. Most studies reported in the literature show that during the reduction process Pd–Cu alloys are formed with Cu segregated onto the surface of the nanoparticles.^{10–14} This selective behavior of Cu is attributed to its lower surface free energy, the exothermicity of the Pd–Cu alloy formation process,

and the strain resulting from the difference in the atomic radii of Cu and Pd.⁹ It has also been reported that the degree of surface segregation of Cu depends on the Cu content of the alloy nanoparticles. No Cu-rich surfaces have been observed in Pd–Cu alloys if the Cu content is low.¹⁴ On the other hand, surface segregation of Pd atoms (reverse segregation) in supported Cu–Pd bimetallic alloys has been reported.^{15–17} This behavior of Pd segregation has been attributed to a strong driving force for dissolution of Cu into Pd. Such a driving force maximizes the Cu–Pd bond formation by gaining the highest possible coordination number for Cu with Pd. It has also been reported that no alloying occurs in alumina-supported Cu–Pd catalysts,¹⁸ even though Cu and Pd can form ordered Cu₃Pd, CuPd, or CuPd₃ phases below 900 K, or disordered alloys over a wide range of composition at high temperatures.¹⁹ These studies indicate that the alloying behavior of bimetallic Pd–Cu catalysts is a complex phenomenon, and the final catalyst structure may strongly depend on the initial metal loadings and the specific reduction process used to make the alloy.

To properly understand the alloying behavior of a bimetallic catalyst system, knowledge of the composition and crystal structure of the metallic phases is critical. Information on the structure and composition of bimetallic catalysts can be obtained by various techniques including EDS,^{6,10,20} high-resolution electron microscopy (HREM),^{6,10,13} and X-ray diffraction (XRD).¹⁷ Furthermore, surface segregation phenomena can be studied by surface-sensitive techniques such as X-ray photoelectron spectroscopy (XPS),^{21,22} Auger electron spectroscopy (AES),^{20,21} infrared spectroscopy (IR),⁶ X-ray absorption spectroscopy (XAS),^{10,11} and low-energy ion spectroscopy (LEIS).¹² However,

* Author to whom correspondence should be addressed: Dr. Kai Sun, Nuclear Engineering & Radiological Sciences, University of Michigan, 2355 Bonisteel Blvd., Ann Arbor, MI 48109-2104. Tel: (734)-764-5290. Fax: (734) 647-8531. E-mail: kaisun@umich.edu.

these techniques do have inherent problems for correctly extracting the surface structure of catalysts. For example, AES or XPS are not strictly surface specific, and the intensity of the detected signal originates from several atomic layers deep into the nanoparticles. XAS provides only the averaged results from a whole sample, thus information on a nanometer or atomic scale, which is important in heterogeneous catalysis, may be missed. Therefore, to understand the alloying phenomenon and surface segregation behavior of the individual bimetallic nanoparticles, new techniques are required to provide high spatial resolution information with high surface and elemental sensitivity.

Scanning transmission electron microscopy techniques can provide cluster-specific alloying information; both atomic resolution Z-contrast imaging^{23–25} and EELS can be performed simultaneously to characterize the composition, structure, and local oxidation state of different materials down to atomic scale.^{26–28} These techniques have been successfully used in the analysis of interfaces and defects,²⁹ and nanoscale clusters in practical catalysts.^{30–33} Moreover, together with the use of the EDS technique, we can extract useful information on the structure/composition/oxidation state profile of individual nanoparticles with subnanometer resolution.

In the present study, we used the above-mentioned atomic scale techniques to examine the alloying behavior of a Pd–Cu/ γ -Al₂O₃ catalyst (containing 2% Pd and 1% Cu), obtained by reducing a Pd–Cu–Al₂O₃ precursor in hydrogen at three different temperatures: 523, 773, and 1073 K. This study builds on our previous investigation of the structure and behavior of supported monometallic catalysts Cu/ γ -Al₂O₃,³² and Pd/ γ -Al₂O₃.³³ The results suggest that the formation of the alloy nanoparticles, their overall composition, and their surface segregation can be understood primarily from the behavior of the individual metal systems.

2. Experimental Procedure

2.1. Catalyst Preparation. Gamma alumina (γ -Al₂O₃) powders (BET SA: 160 m²/g, and Hg pore vol 2.3 mL/g) were used as the support. Sufficient amounts of aqueous solutions of Na₂PdCl₄ and CuCl₂·2H₂O were mixed together (to give a catalyst containing 2% Pd and 1% Cu) and the pH was adjusted to 4. This mixture was added dropwise to a 10% slurry (The pH of the slurry was adjusted to 11 by sodium carbonate) of the alumina powder with constant stirring by an impeller. After 30 min of adsorption of the salt, the temperature was raised to 338 K, and held at this temperature while being stirred for another 30 min. After complete adsorption of the salt, as indicated by clear filtrate from the slurry, the solid was filtered, washed, and dried overnight at 393 K. Portions of this dry material were reduced at three different temperatures, 523, 773, and 1073 K, as follows. The catalyst was loaded in a tubular furnace and protected by two plugs of quartz wool. A thermocouple was placed in the center of the catalyst bed. The air was flushed with nitrogen, and replaced by a flow of 4% H₂ in Ar (40 mL/min). The temperature was slowly raised to the desired final value and then held at this temperature for 2 h. The catalyst was then cooled to room temperature in hydrogen, discharged into containers, and packed without being prevented from air exposure. Specimens for electron microscopy analysis were prepared by placing the powders on holey-carbon-coated Mo grids directly.

2.2. Electron Microscopy and Spectroscopy. A JEOL 2010F 200kV Schottky field emission STEM/TEM equipped with a thermo Noran Vantage EDX system (Voyage) (with a 40 mm²

atmospheric thin window Si(Li) detector) and a Gatan PEELS system was used for the experimental analysis described here. The lens conditions in the microscope for EELS and Z-contrast imaging were defined for a probe size of about 0.2 nm, with a convergence angle of 13 mrad and a collection semi-angle of 52 mrad for the annular dark-field detector. The energy resolution of the energy-loss spectra is about 1.2 eV (defined by the full width at half-maximum (fwhm) of zero loss peak) at a dispersion of 0.3 eV/channel. All the core-loss spectra were acquired using a 3 s dwelling time. A detailed description of the techniques has been given elsewhere.^{23,30} What we should mention here is that for each samples we have analyzed several particles from several different areas and specimens. The following results are just examples of each case. For EDS, which was performed both in spot and scanning modes, the lens conditions were defined for a probe size of 0.5 nm to have adequate probe current.

3. Results

3.1. Size and Size Distribution of the Nanoparticles. Figure 1a is a Z-contrast image showing the overall morphology of the catalyst reduced at 523 K. This image shows that many small particles are formed during the reduction–calcination process. To obtain the particle size distribution, 200 particles in several Z-contrast images taken from different areas and from different TEM specimens (all produced by the same method) were measured. The particle size distribution in Figure 1b shows that nearly half of the particles formed are in the size range of 3–5 nm. No more than 10 percent of the particles were larger than 10 nm. This size distribution is similar to that observed for a Pd/ γ -Al₂O₃ catalyst reduced at the same temperature.³³ On the other hand, there were no observable metal particles in the Cu/ γ -Al₂O₃ catalyst made and reduced at the same temperature.³²

Figure 1c is a Z-contrast image of the catalyst reduced at 773 K. The particle size distribution was determined in the same manner as for the 523 K sample and is shown in Figure 1d. This size distribution indicates that more than sixty percent of the particles are in the size range of 3–5 nm and the particle size distribution in the catalyst reduced at 773 K seems to be more homogeneous. This narrower distribution is again somewhat similar to what was observed with the Pd/ γ -Al₂O₃³³ catalyst as mentioned earlier. On the other hand, the analysis of the Cu/ γ -Al₂O₃³² showed that the majority of the Cu particles formed at 773 K were in the 10–15 nm size range.

Figure 1e is a representative Z-contrast image taken from the catalyst reduced at 1073 K. The size distribution shown in Figure 1f shows that the particles reduced at higher temperature have grown into the size range of 10–40 nm (~80%) with a few very large (around 100 nm or larger) and some small particles (smaller than 10 nm). Previous studies of both the Pd/ γ -Al₂O₃³³ and the Cu/ γ -Al₂O₃³² systems showed similar size distributions.

3.2. Composition of the Individual Nanoparticles. We used EDS technique to obtain the compositional profiles of the individual particles formed during the reduction process. For the catalysts reduced 523 and 773 K, about 30 particles from different areas and specimens were analyzed, respectively (see Table 1). For the catalyst reduced at 523 K, both pure metallic Pd particles (about 20% of the particles) and alloyed particles consisting of both Pd and Cu with a wide compositional range were formed. Neither Pd nor Cu peaks were seen in the EDS spectrum collected from the support only. (This is also the case for the samples reduced at 773 and 1073 K.). In the sample reduced at 773 K, there are still about 15% pure Pd particles

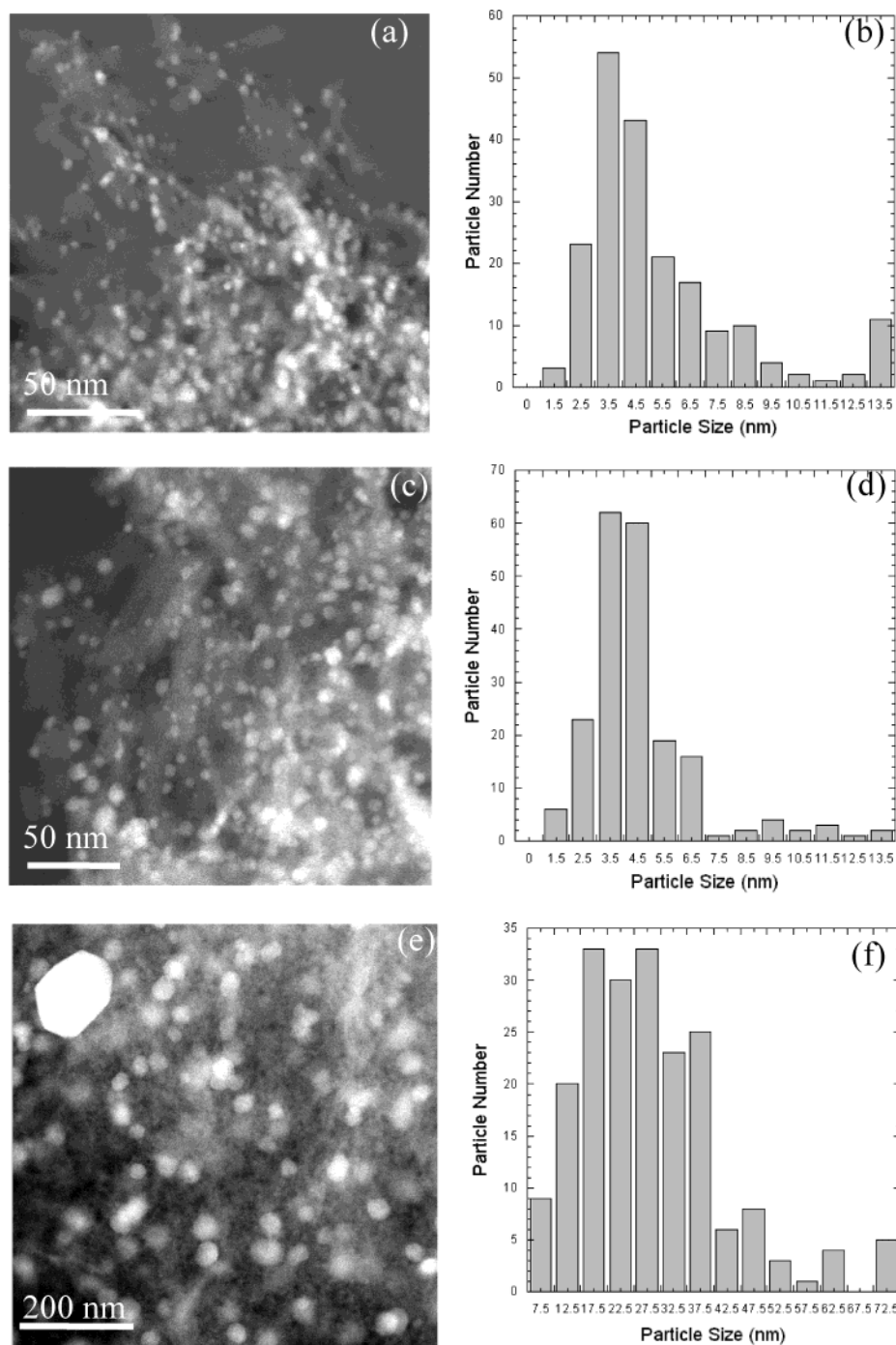


Figure 1. (a), (c), and (e) are low-magnification Z-contrast images of the catalyst reduced at 523, 773, and 1073 K, respectively; (b), (d), and (f) are histograms showing the formed particle size distribution of the catalyst reduced at these three different temperatures, respectively.

present in the catalyst. For the catalyst reduced at 1073 K, measurement of about fifty particles (only 30 were showed in Table 1) showed that most of them (>90%) had compositions such as Pd₆₇Cu₃₃, Pd₅₀Cu₅₀, or Pd₃₃Cu₆₇. Our results obtained here are consistent with the results obtained by Haller and co-workers.¹⁸ These results suggest that at temperatures of 773 K or below, Pd and Cu have not been completely alloyed. This is consistent with the size distributions for the particles shown in Figure 1 that exhibit features consistent with the monometallic catalysts.³³

3.3. Element Distribution and Oxidation States. EELS and Z-contrast imaging were used to determine the distribution of the metals within the individual bimetallic nanoparticles. Figure 2a shows a representative Z-contrast image taken from the

catalyst reduced at 523 K. (Note: In this paper we will not present results from the pure Pd particles as they show the same features as those observed in the Pd/ γ -Al₂O₃ catalyst examined previously.³³) In this image a metal particle is observed to be sitting on a support. Palladium and copper core-loss spectra acquired from the specific sites in Figure 2a are shown in Figure 2b,c. These core-loss spectra were processed by subtracting backgrounds from the experimental spectra via fitting the preedge to a power law function of the form AE^{-r} (where E is the energy loss, A and r are constants).³⁴ The spectra have been normalized to the continuum interval between 570 and 600 eV and 1070–1100 eV, respectively, and then shifted vertically for clarity. Due to the lower counts in the Cu:L_{2,3} edge, the displayed spectra were smoothed to alleviate the noise level. It

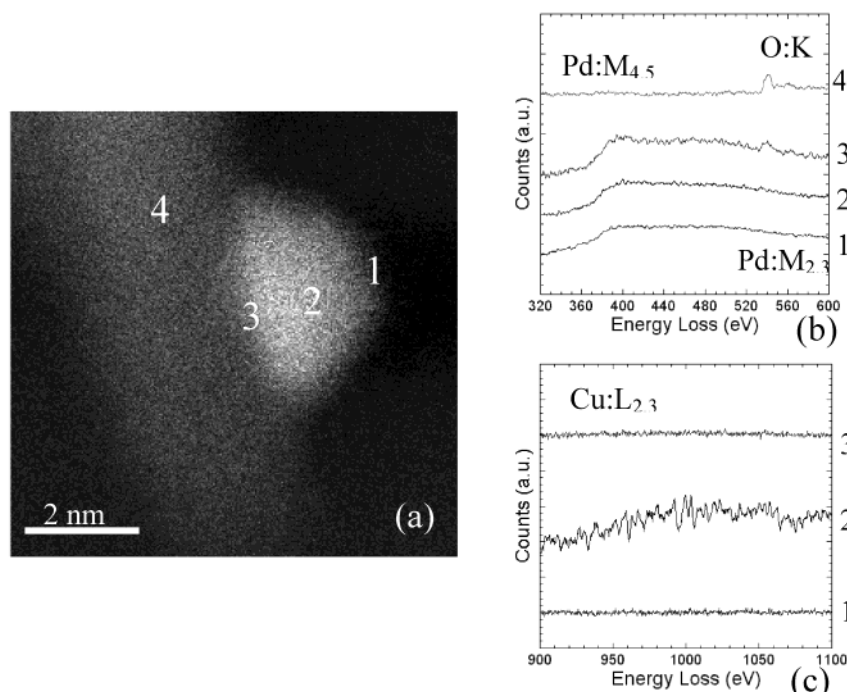


Figure 2. (a) Z-contrast image taken from the catalyst reduced at 523 K; and (b) and (c) corresponding EEL Pd and Cu core-loss spectra acquired from the specific sites marked in (a).

TABLE 1: Compositions of Particles Formed in the Catalyst Reduced at Different Temperatures

reduction temperature (K)	content of Pd (at. %)	no. of particles
523	100	6
	70–90	4
	50–70	16
	30–50	4
773	100	4
	70–90	5
	50–70	13
	30–50	5
1073	100	0
	70–90	0
	50–70	18
	30–50	12

is observed that spectra **1** and **2** in Figure 2b consist of delayed Pd:M_{4.5} (335 eV), Pd:M_{2.3} (532.3 eV) edges, which suggests that Pd exists in metallic Pd state in the particle (consistent with the observations from Pd/γ-Al₂O₃). The O:K (532 eV) peak in spectrum **3** (acquired from the interface) originates from the alumina support. There were no Cu:L_{2,3} (931 eV) peaks present in spectra **1** and **3** as shown in Figure 2c, indicating that the surface of the particle primarily consists of Pd. In spectrum **2**, a Cu signal is observed with a fine-structure consistent with metallic Cu.³⁵ The EELS data therefore clearly show that this particle has a metallic Pd shell and a Pd–Cu alloy (Pd/Cu = 1/1 from the EEL spectra) core.

Figure 3a shows another Z-contrast image of the catalyst reduced at 523 K, taken from another area in which three distinct particles supported on alumina are seen. Palladium and copper core-loss spectra acquired from the marked sites in the image are shown in Figure 3b,c. These spectra were processed in the same manner as above. All the spectra in Figure 3b contain Pd core-loss edges besides O:K edges from the support. (The particles are on the surface of the support in this orientation so that the oxygen signal is always present.) Cu:L_{2,3} edges (metallic Cu³⁵), however, only show up in spectra **1**, **3**, **4**, and **5**. This

indicates that the particle marked as **1** is a Pd–Cu bimetallic alloy, whereas the particle marked as **6** is pure metallic Pd. The composition of the particle lying between the two particles is nonuniform, containing regions of pure metallic Pd and regions of a bimetallic Pd–Cu alloy.

In Figure 4a, a particle formed in the catalyst reduced at 773 K is shown. The corresponding Pd and Cu core-loss spectra acquired from the specific sites **1**, **2**, and **3** are shown in Figure 4b and 4c, respectively. These spectra were processed in the same manner as the previous spectra. Given that metallic Pd:M edges show up in all the spectra while metallic Cu:L_{2,3} only show up in spectrum **2**, we conclude that this particle has a pure metallic Pd shell and a Pd–Cu alloy core (Pd/Cu = 1/1 from the EEL spectra).

Another particle formed in the catalyst reduced at 773 K is shown in Figure 5a. Processed Pd and Cu core-loss spectra acquired from the specific sites marked in Figure 5a are shown in Figure 5b,c. Analyses of these spectra indicate that this is a completely alloyed Pd–Cu bimetallic particle with possibly more Pd segregated to the surface. For positions **1**, **3**, and **5**, quantification of the spectra gives Pd/Cu ratios of about 3.2/1, 1/1, and 1.2/1, respectively.

Figure 6a shows a particle in the catalyst reduced at 1073 K. Pd and Cu core-loss spectra were acquired from the specific sites marked in the particle shown in Figure 6b and 6c, respectively. These spectra indicate that the particle contains metallic Pd and Cu and thus is a totally alloyed Pd–Cu bimetallic particle. Quantification of these spectra shows that there is a surface enrichment of Pd in the particle. We should mention that some particles with Cu-enrichment in the surfaces were also detected, which is consistent with the observation of Cu-rich particles by EDS measurement. To obtain the two-dimensional elemental distributions within the particles formed at this temperature, EDS elemental mapping was performed in several different areas of the sample. Figure 7 shows an EDS elemental map, which contains Pd, Cu, and Al maps and the corresponding Z-contrast image. The elemental maps clearly show that all the nanoparticles are Pd–Cu bimetallic alloys.

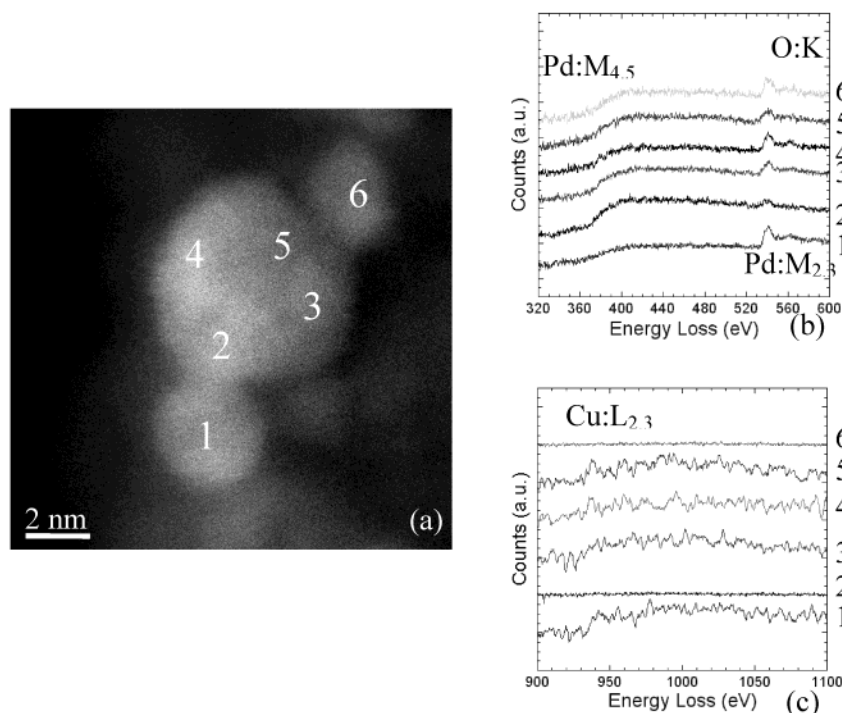


Figure 3. (a) Z-contrast image taken from the catalyst reduced at 523 K; and (b) and (c) corresponding EEL Pd and Cu core-loss spectra acquired from the specific sites marked in (a).

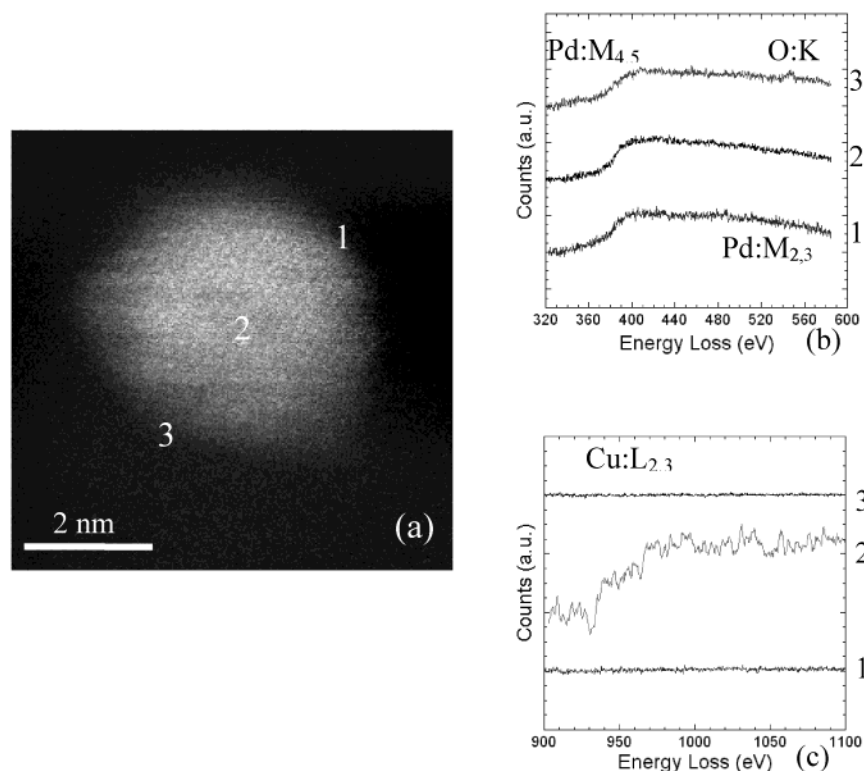


Figure 4. (a) Z-contrast image taken from the catalyst reduced at 773 K; and (b) and (c) corresponding EEL Pd and Cu core-loss spectra acquired from the specific sites marked in (a).

Electron energy loss spectroscopy analysis also revealed chemical shifts in the spectra acquired from the interfaces between the bimetallic alloys and the support. For example, a 2.1 eV chemical shift between the spectrum 3 and 4 (acquired from the alumina support) in Figure 2b is observed. No chemical shifts were observed in the spectra acquired from the interfaces between pure metallic Pd particles and the support. This is consistent with the previous analysis of Pd/ γ -Al₂O₃.³³

where chemical shifts were only observed for the larger particles, ~ 10 nm in size. In the Cu–Pd/ γ -Al₂O₃ system studied here, all larger particles are bimetallic.

4. Discussion

The above results clearly show that Pd and Cu are alloyed in the Pd–Cu/ γ -Al₂O₃ catalyst when reduced at higher temperatures, and this is consistent with the reports on supported Pd–

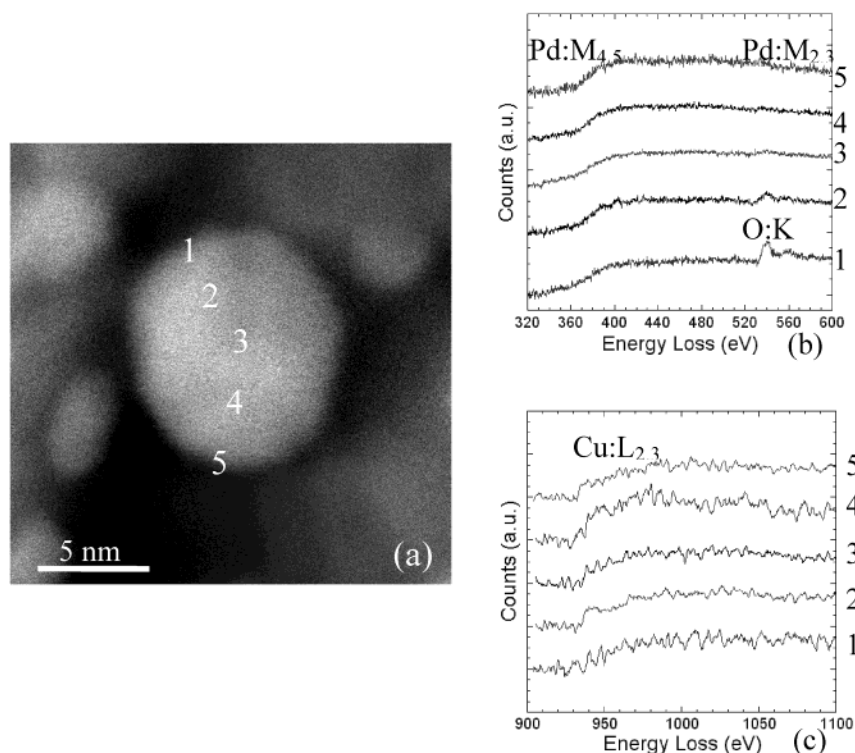


Figure 5. (a) Z-contrast image taken from the catalyst reduced at 773 K; and (b) and (c) corresponding EEL Pd and Cu core-loss spectra acquired from the specific sites marked in (a).

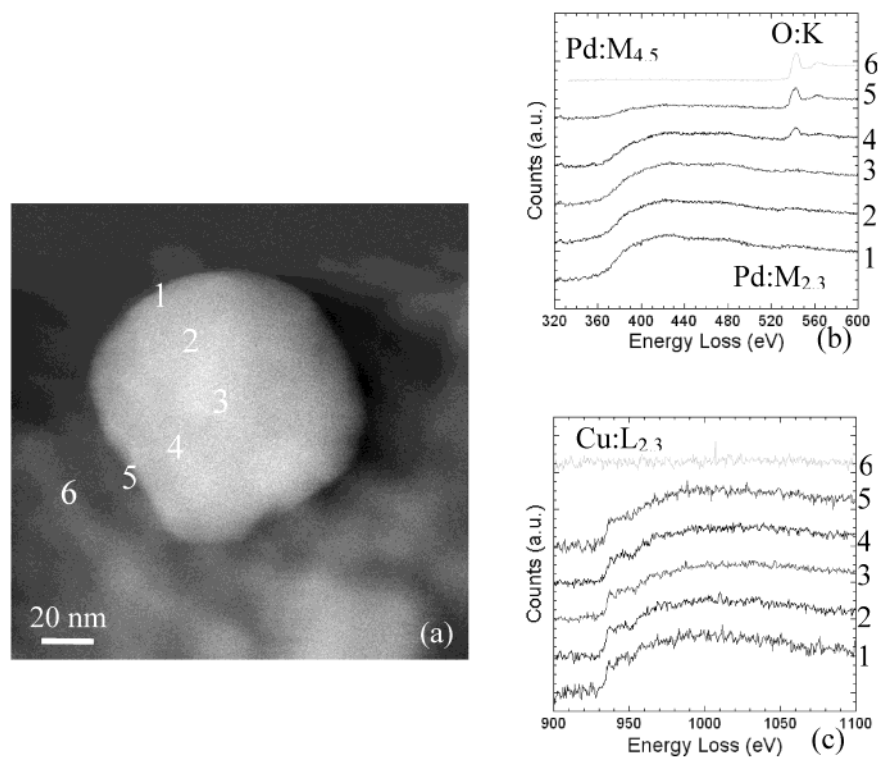


Figure 6. (a) Z-contrast image taken from the catalyst reduced at 1073 K; and (b) and (c) corresponding EEL Pd and Cu core-loss spectra acquired from the specific sites marked in (a).

Cu systems.^{8–10,12,13} By considering the structural evolution of the particles at different temperatures, the formation of these Pd–Cu alloys can be evaluated. It can be speculated that, during reduction at temperatures lower than 773 K, Pd is first reduced and sinters into separated particles. Following this, the reduced Cu species diffuse into the Pd particles at higher reduction temperatures, resulting in the formation of bimetallic Pd–Cu

particles. Particles with a low Cu content tend to have a metallic Pd shell and Pd–Cu alloy core structures, and this indicates that the reverse segregation phenomenon, observed in other supported Pd–Cu systems,^{15–17} has occurred in these Pd–Cu/ γ -Al₂O₃ catalysts. The small bimetallic particles with a wide range of compositions formed at low reduction temperatures eventually sinter into large bimetallic particles at high reduction

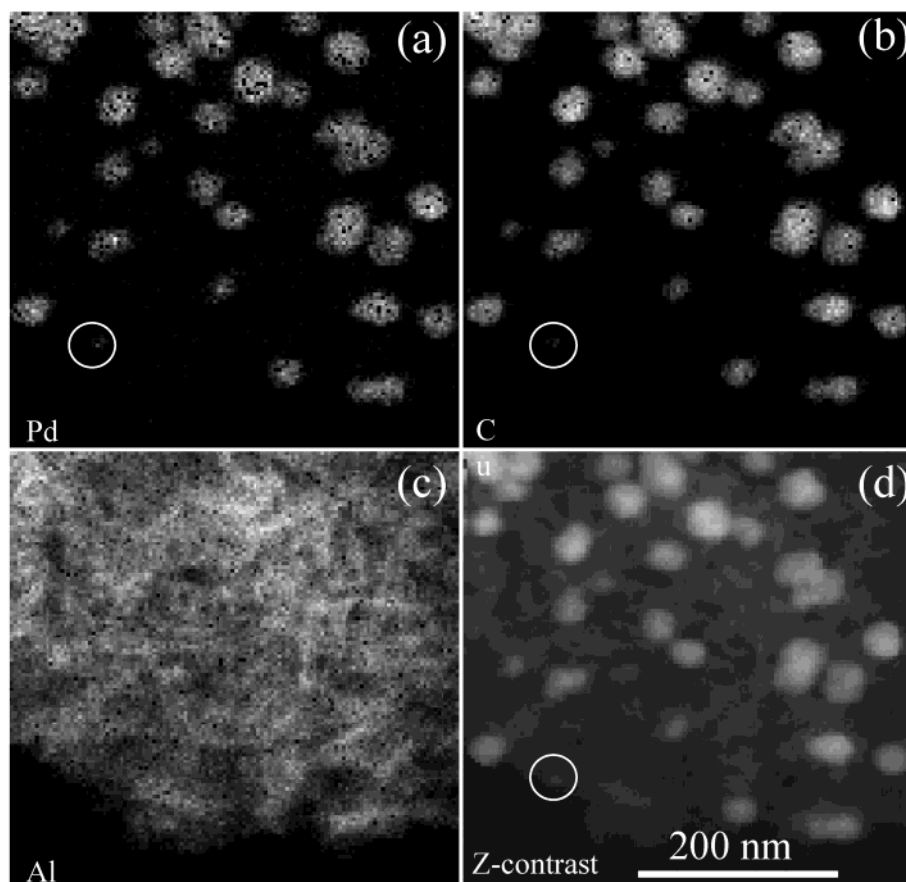


Figure 7. EDS elemental maps show the distribution of Pd, Cu, and Al in the catalyst reduced at 1073 K (performed at a magnification of 200 000 times for 88.7 min with the image size of 128 \times 128 pixels).

temperatures. Since the diffusion and sintering processes are nonuniform, bimetallic particles with different compositions are formed. These bimetallic Pd–Cu particles may consist of either Pd- or Cu-enriched surfaces. However, since Cu can dissolve into PdO up to 15 mol %, ³⁶ mixed Pd–Cu oxides might also have formed before reduction, and as a result some Pd–Cu bimetallic particles may have formed from the reduction of mixed Pd–Cu oxides directly. Further studies using in-situ environmental electron microscopy techniques may provide more insight into the reduction and the formation processes of bimetallic nanoparticles.

In the previous study on Cu/ γ -Al₂O₃ catalysts, we found that when reduced at temperatures below 773 K, copper oxide species had not completely been reduced.³² In the present situation, bimetallic particles containing metallic Cu were formed even at temperatures as low as 523 K, suggesting that Pd may enhance the reduction of copper species.³⁷ By comparing to the results obtained from the Pd/ γ -Al₂O₃³³ system, we found that the presence of Cu did not decrease the size of the nanoparticles. This is not consistent with that reported in the literature that Cu enhances the stability of the metal particles against sintering.¹⁴

No chemical shift was detected between pure metallic Pd particles smaller than 5 nm in the Pd/ γ -Al₂O₃ catalysts while chemical shifts (Pd:M edge shifts³³) were observed for bimetallic Pd–Cu particles within this size range. This might be due to the modification of the Pd electronic structure by Cu in the bimetallic Pd–Cu catalyst. It has been reported that after alloying, the electron density of Pd metal is increased due to electron transfer from copper to palladium.³⁸ However, the reported chemical shift due to alloying between Pd and Cu is

no more than 1 eV,²¹ so the 2.1 eV chemical shift mentioned previously may also contain a contribution of charge transfer from the support (alumina) to the Pd–Cu particles. The addition of Cu in the particle therefore appears to enhance the metal support interaction (MSI) via electronic modification of Pd by Cu. Further experiments to probe the electron-transfer mechanisms are in progress and will be reported later.

5. Conclusions

In summary, the formation of Pd–Cu bimetallic nanoparticles with nonhomogeneous distribution of both elements is observed in a Pd–Cu/Al₂O₃ catalyst. In particular, at reduction temperatures below 773 K, pure metallic Pd, Pd–Cu bimetallic particles with Pd segregated to the surface and with mixed layer termination (over a wide range of compositions) are formed. When the catalyst precursor is reduced at 1073 K, large particles of bimetallic alloys with either Pd-rich or Cu-rich surfaces are observed. Alloy nanoparticles with varying composition and surfaces segregation are also formed during reduction at high temperatures. The addition of Cu appears to enhance charge transfer or MSI.

Acknowledgment. This research was sponsored by Monsanto Company and the Petroleum Research Fund. The JEOL 2010F STEM/TEM used in this research was partially funded by NSF through Grant DMR-9601792 and is operated by the Research Resources Center at UIC.

References and Notes

- (1) Sinfelt, J. H. *Bimetallic Catalysts, Discoveries, Concepts and Applications*; Wiley: New York, 1983.

- (2) Coq, B.; Figueras, F. *J. Mol. Catal. A* **2001**, 173, 117.
- (3) Hörold, S.; Vorlop, K. D.; Tacke, T.; Sell, M. *Catal. Today* **1993**, 17, 21.
- (4) Rodriguez, J. A.; Goodman, D. W. *Science* **1992**, 257, 897.
- (5) Sachtler, W. M. H.; van Santen, R. A. *Adv. Catal.* **1997**, 26, 69.
- (6) Reyes, P.; Figueroa, A.; Pecchi, G.; Fierro, J. L. G. *Catal. Today* **2000**, 62, 209.
- (7) Fernández-García, M.; Martínez-arias, A.; Belver, C.; Anderson, J. A.; Conesa, J. C.; Soria, J. *J. Catal.* **2000**, 190, 387.
- (8) Ilinitich, O. M.; Cuperus, F. P.; Nosova, L. V.; Gribov, E. N. *Catal. Today* **2000**, 56, 137.
- (9) Bardi, U. *Rep. Prog. Phys.* **1994**, 57, 939.
- (10) Batista, J.; Pintar, A.; Gomilšek, J. P.; Kodre, A.; Bornette, F. *Appl. Catal. A* **2001**, 217, 55.
- (11) Edelmann, A.; Schießer, W.; Vinek, H.; Jentys, A. *Catal. Lett.* **2000**, 69, 11.
- (12) Renouprez, A. J.; Lebas, K.; Bergeret, G.; Rousset, J. L.; Delichère, P. *Stud. Surf. Sci. Catal.* **1996**, 101, 1105.
- (13) Molenbroek, A. M.; Haukka, S.; Clausen, B. S. *J. Phys. Chem.* **1998**, B102, 10680.
- (14) Fernández-García, M.; Anderson, J. A.; Haller, G. L. *J. Phys. Chem.* **1996**, 100, 16247.
- (15) Bradley, J. S.; Hill, E. W.; Chaudret, B.; Duteil, A. *Langmuir* **1995**, 11, 693.
- (16) Bradley, J. S.; Via, G. H.; Bonneviot, L.; Hill, E. W. *Chem. Mater.* **1996**, 8, 1895.
- (17) Toshima, N.; Wang, Y. *Langmuir* **1994**, 10, 4574.
- (18) Strukul, G.; Pinna, F.; Marella, M.; Meregalli, L.; Tomaselli, M. *Catal. Today* **1996**, 27, 209.
- (19) Villards, A. P.; Calvet, L. D. *Pearson's Handbook of Crystallographic Data for Bimetallic Phases*; ASM Int.: Materials Park, OH, 1991.
- (20) Batista, J.; Pintar, A.; Čeh, M. *Catal. Lett.* **1997**, 43, 79.
- (21) Mårtensson, N.; Nyholm, R.; Calén, H.; Hedman, J. *Phys. Rev. B* **1981**, 24, 1725.
- (22) Polak, M.; Rubinovich, L. *Surf. Sci. Rep.* **2000**, 38, 127.
- (23) Treacy, M. M. J.; Howie, A.; Wilson, C. J. *Philos. Mag. A* **1978**, 38, 569.
- (24) Liu, J.; Cowley, J. M. *Ultramicroscopy* **1990**, 34, 119.
- (25) Nellist, P. D.; Pennycook, S. J. *Science* **1996**, 274, 413.
- (26) Browning, N. D.; Chisholm, M. F.; Pennycook, S. J. *Nature* **1993**, 366, 143.
- (27) Batson, P. E. *Nature* **1993**, 366, 727.
- (28) James, E. M.; Browning, N. D. *Ultramicroscopy* **1999**, 78, 125.
- (29) Xin, Y.; James, E. M.; Arslan, I.; Sivananthan, S.; Browning, N. D.; Pennycook, S. J.; Omnes, F.; Beaumont, B.; Faurie, J. P.; Gibart, P. *Appl. Phys. Lett.* **2000**, 76, 466.
- (30) Sun, K.; Liu, J.; Browning, N. D. *J. Catal.* **2002**, 205, 266.
- (31) Klie, R. F.; Disko, M. M.; Browning, N. D. *J. Catal.* **2002**, 205, 1.
- (32) Sun, K.; Liu, J.; Browning, N. D. *Appl. Catal. B* **2002**, 38, 271.
- (33) Sun, K.; Liu, J.; Nag, N.; Browning, N. D. Studying the Metal-Support Interaction in Pd/ γ -Al₂O₃ Catalysts by Atomic-Resolution Electron Energy Loss Spectroscopy. *Catal. Lett.*, accepted for publication.
- (34) Egerton, R. F. *Electron Energy Loss Spectroscopy in the Electron Microscope*, 2nd ed.; Plenum: New York, 1996.
- (35) Ito, Y.; Jain, H.; Williams, D. B. *Appl. Phys. Lett.* **1999**, 75, 3793.
- (36) Niu, C.-M.; Rieger, P. H.; Dwight, K.; Wold, A. *J. Solid State Chem.* **1990**, 86, 175.
- (37) Fernández-García, M.; Conesa, J. C.; Clotet, A.; Ricart, J. M.; López, N.; Illas, F. *J. Phys. Chem. B* **1998**, 102, 141.
- (38) Noronha, F. B.; Primet, M.; Frety, R.; Schmal, M. *Appl. Catal.* **1991**, 78, 125.